Since January 2020 Elsevier has created a COVID-19 resource centre with free information in English and Mandarin on the novel coronavirus COVID-19. The COVID-19 resource centre is hosted on Elsevier Connect, the company's public news and information website.

Spectrochimica Acta Part A: Molecular and Biomolecular Spectroscopy 264 (2022) 120237

Contents lists available at ScienceDirect

Spectrochimica Acta Part A: Molecular and Biomolecular Spectroscopy

journal homepage: www.elsevier.com/locate/saa

Synthesis of gold nanoparticles@reduced porous graphene-modified ITO electrode for spectroelectrochemical detection of SARS-CoV-2 spike protein

Waleed A. El-Said *, Abdullah S. Al-Bogami, Wael Alshitari

Department of Chemistry, College of Science, University of Jeddah, P.O. Box 80327, Jeddah 21589, Saudi Arabia

HIGHLIGHTS

- Au NPS/porous graphene modified ITO electrode was used as a COVID-19 biosensor.
- The spectroelectrochemical biosensor was used to monitor the COVID-19 S protein.
- The developed sensor showed a lower detection limit of 39.5 fmol L^{-1}.
- The spectroelectrochemical sensor is based on SERS, CV and SWV techniques.

GRAPHICAL ABSTRACT

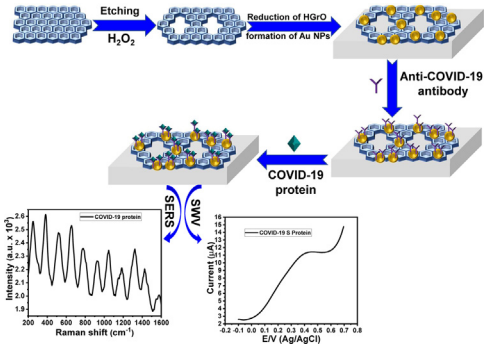

ARTICLE INFO

Article history:
Received 4 May 2021
Received in revised form 1 July 2021
Accepted 26 July 2021
Available online 28 July 2021

Keywords:
Gold nanoparticles
Reduced porous graphene oxide modified ITO electrode
Surface enhanced-Raman spectroscopy
COVID-19
Square wave voltammetry
Spectroelectrochemical biosensor

ABSTRACT

Here, we reported the synthesis of reduced porous graphene oxide (rPGO) decorated with gold nanoparticles (Au NPs) to modify the ITO electrode. Then we used this highly uniform Au NPs@rPGO modified ITO electrode as a surface-enhanced Raman spectroscopy-active surface and a working electrode. The uses of the Au nanoparticles and porous graphene enhance the Raman signals and the electrochemical conductivity. COVID-19 protein-based biosensor was developed based on immobilization of anti-COVID-19 antibodies onto the modified electrode and its uses as a probe for capturing the COVID-19 protein. The developed biosensor showed the capability of monitoring the COVID-19 protein within a concentration range from 100 nmol/L to 1 pmol/L with a limit of detection (LOD) of 75 fmol/L. Furthermore, COVID-19 protein was detected based on electrochemical techniques within a concentration range from 100 nmol/L to 500 fmol/L that showed a LOD of 39.5 fmol/L. Finally, three concentrations of COVID-19 protein spiked in human serum were investigated. Thus, the present sensor showed high efficiency towards the detection of COVID-19.

1. Introduction

Several coronavirus strains were identified, including SARS-CoV, HCoV-229E, HCoV-OC43, HCoVHKU1, and MERS-CoV [1]. In addition, a new coronavirus (COVID-19) has reported at the end of 2019 [2-6]. The COVID-19 has fast spread worldwide in a short time compared with other coronaviruses [5,6]. However, the early diagnosis is difficult because there are no initial characteristic symptoms of COVID-19 in the early stage of infection; besides, many cases did not show the common signs [7]. Thus, there is an

* Corresponding author.
E-mail address: waahmed@uj.edu.sa (W.A. El-Said).

https://doi.org/10.1016/j.saa.2021.120237
1386-1425/

urgent need to find antiviral drugs besides developing an accurate, simple, and sensitive sensing method.

The real-time reverse transcription-polymerase chain reaction (rRT-PCR) is the golden technique for detecting COVID-19. However, its costly, needs specialist laboratories, skilled persons, and consumed a long time, which has limited their use [8,9]. Thus, it is of great urgency to develop rapid, reproducible, cost-effective, easy-to-use, accurate, sensitive, and selective assays for the early diagnosis of COVID-19 in different specimens.

Therefore, it is urgently needed to develop cost-effective, easy-to-use, fast, accurate, sensitive, selective, and real-time detection assays for the early diagnosis of COVID-19 infection. Biosensors have several advantages, such as the rapid response and the high sensitivity and selectivity towards many biological species. Raman spectroscopy is one of the promising labelless, specific, accurate, sensitive, and nondestructive assays. Raman's specificity is related to the fact that Raman showed fingerprints biochemical composition of the analyzed samples. Thus, Raman spectroscopy is one of the most promising techniques for real-time detection of different biological samples without sample preparation. However, the weak Raman signals are the main disadvantaged of Raman spectroscopy as a comprehensive analytical technique. Surface-enhanced Raman scattering (SERS) is one of the widely used methods to overcome this inherent limitation and enhance the signals' strength based on the uses of nanostructured metallic surfaces (gold and silver) [10,11]. Hence, SERS has widely used for biosensing applications [12-19].

Furthermore, electrochemical biosensors detect the most easy-to-use, accurate, quick, and sensitive biomarkers [14,20,21]. Several nanostructures modified electrodes have been reported to enhance the sensitivity and selectivity of the electrochemical biosensors [22-28]. MWCNTs modified electrode was also used as an electrochemical sensor for detecting the ROS/H_2O_2 in the COVID-19 samples. Hence, it could use for the early-stage screening, which showed a good agreement between the electrochemical results and the clinical diagnostics [29].

Besides the exclusive properties of the graphene-based materials [30-32]. Graphene is an extraordinary 2D material that can enhance the electrochemical conductivity of the traditional electrodes and enhance the Raman effect based on graphene-enhanced Raman scattering (GERS) [30,31]. Moreover, metals nanostructures have wildly reported for improving the electrochemical conductivity and the Raman scattering. Thus, the graphene/metal NPs hybrids could improve the graphene/metal nanocomposites' electrical conductivity compared with the pure graphene or metal NPs [32,33]. Thus, these nanocomposites have shown promising applications in several fields, including catalysis, energy conversion, and chemo/biosensors [32,33].

Here, we have reported on the uses of the Au NPs@reduced porous graphene oxide (rPGO) modified ITO substrate as a SERS-active surface and act as a scaffold for immobilization of the anti-COVID-19 antibodies. Besides, we have used these Au NPs decorated rPGO to improve the Raman signals and the electrochemical conductivity. The anti-COVID-19 antibodies were used as probes for monitoring the COVID-19 based on Raman spectroscopy, cyclic voltammetry (CV), and square wave voltammetry (SWV) techniques. This spectroelectrochemical biosensor showed a capability to detect the COVID-19 protein within a concentration range from 100 nmol/L to 500 fmol/L with a limit of detection (LOD) of 39.5 fmol L^{-1} based on the SWV technique. Finally, this spectroelectrochemical sensor was used to detect different concentrations of COVID-19 protein in human serum samples that showed a good recovery percentage.

2. Experimental details

2.1. Materials and reagents

Chloroauric acid ($H_3AuCl_4{\cdot}4H_2O$), ascorbic acid, and phosphate buffer saline (PBS) (1x, pH = 7.4) were purchased from Sigma-Aldrich (St. Louis, MO, USA). Graphene oxide (GO) nanosheets were obtained from Graphene Supermarket (Ronkonkoma, New York 11779, USA) as a suspension in water. COVID-19 antibody (S1N-M122, monoclonal antibody, IgG1) and COVID-19 S1 protein (S1N-C52H2, MWt = 76.9 kDa) were purchased from ACROBiosystems (Newark, Delaware, USA). All other chemicals were analytical-grade reagents.

2.2. Preparation of porous graphene oxide (PGO)

PGO was prepared based on the etching method by using an H_2O_2 solution. Typically, 50 mL of 1 mg/mL GO sheets suspension was mixed with 5 mL of H_2O_2 (30 %) aqueous solution. The mixture was dispersed by sonication for 30 min and then heated at 100 °C for 4 h. Next, the PGO was obtained by centrifuging, and the residual of H_2O_2 was removed by washing the PGO with DIW. Finally, the PGO was re-dispersed in DIW by ultrasonication for 20 s.

2.3. Preparation of reduced porous graphene oxide (rPGO)

RPGO was prepared by using ascorbic acid as a reducing agent. Typically, 0.5 mL of 1 M ascorbic acid was mixed with 10 mL 1 mg/mL PGO and then heated for 2 h at 100 °C. The rPGO was purified by using DIW.

2.4. Preparation of Au nanoparticles/reduced porous graphene and its modified ITO electrode

Au NPs@rPGO was prepared under the same condition as the rPGO but in the presence of chloroauric acid. Typically, 1 mL of PGO (1 mg/mL) was mixed with 50 mM of $HAuCl_4$ (1 mmol L^{-1}) aqueous solution and 0.5 mL of 1 M ascorbic acid and then heated at 100 °C for 1 h. The rPGO was obtained by centrifuge and dried at room temperature. Furthermore, Au NPs@rPGO modified ITO substrates were also prepared according to the same condition but by insert ITO (0.5 cm × 2 cm) inside the reaction's vessel and keeping the conducting surface upward.

2.5. Fabrication of the COVID-19 spectroelectrochemical sensor

Au NPs@rPGO modified ITO substrate was cleaned by rinsed with ethanol and dried under an N_2 stream. Next, a 50 μL of the anti-COVID-19 antibody (10 μg/ml) in a 10 mM PBS buffer was immobilized onto the ITO substrate and kept overnight at 4 °C. We then rinsed the substrates three times using 1x PBS. Subsequently, 50 μL of COVID-19 protein solutions with different concentrations were interacted with the anti-COVID-19 antibody/Au NPs@rPGO modified ITO substrate for a further 1 h at 4 °C. Finally, the substrate was washed with 10 mM PBS and DIW and dried under N_2 gas.

2.6. Instruments

The SERS spectra were collected on Raman spectroscopy with a SENTERRA inverted confocal Raman microscope (Bruker Optics Inc., Germany) comprises a CCD camera detection system and OPUS software for data acquisition. The spectra were recorded using NIR laser emitting light at a wavelength of 785 nm and a power of 50 mW at the sample. Ten scans of 5 s from 500 cm^{-1}

to 2000 cm^{-1} were recorded, and the average data were represented.

Furthermore, the AUTOLAB electrochemical workstation instrument (Metrohm, Herisau, Switzerland) was used to record the electrochemical data. A three-electrode-based homemade electrochemical cell consisting of Ag/AgCl as the reference electrode, anti-COVID antibodies/Au NPs/rPGO modified working electrode, and Pt wire auxiliary electrode was reported. All the electrochemical measurements were performed in 10 mM PBS (pH = 7,4) electrolyte within the potential window from −0.1 V to +0.7 V at a scan rate of 50 mV/s.

The surface morphology of reduced porous graphene and Au NPs decorated reduced porous graphene-modified ITO substrates were analyzed by a scanning electron microscope (SEM) (ISI DS-130C, Akashi Co., Tokyo, Japan).

2.7. Sensing of COVID-19 in spiked samples

To prepare a representative of the real model, we have admixed different concentrations of the COVID-19 protein with 50 μg human serum. About 50 μL of the mixture was directly immobilized onto antiCOVID-19 antibody/Au NPs decorated reduced porous graphene/ITO for about 6 h at room temperature. Finally, the substrate was directly used to investigate the COVID-19 protein based on SERS, CV, and SWV techniques.

3. Results and discussion

3.1. Fabrication of COVID-19 biosensor based on SERS technique

Here, we have developed a simple, easy, and nondestructive COVID-19 spectroelectrochemical biosensor based on the SERS and electrochemical techniques, as shown in Scheme 1. The sensing process utilizes the Au NPs@rPGO modified electrode as a SERS-active surface and a working electrode. Firstly, we synthesized porous graphene sheets based on the treatment of GO sheets with H_2O_2. Fig. 1**a** showed the SEM image of PGO, which showed the fabrication of highly uniform porous GO sheets over a large area. Then, simultaneously PGO was reduced to form rPGO, and Au NPs were formed by using ascorbic acid as a reducing agent. Fig. 1**b** showed the SEM image of Au NPs@rPGO that illustrated the formation of spherical Au NPs with a diameter of about 100 nm.

Furthermore, the formation of rPGO was confirmed using Raman spectroscopy (Fig. 1**c**), which showed the characteristics of G and D Raman bands of the graphene. Both Raman signals and electrochemical conductivity will be enhanced based on both Au NPs (noble metal NPs) and graphene material (2D material). The development of the COVID-19 sensor, including the immobilization of anti-COVID-19 antibody onto the Au NPs@rPGO modified ITO, followed by the capturing of the COVID-19 protein with the anti-COVID-19 antibody and monitoring this interaction based on the SERS and electrochemical techniques.

3.2. SERS detection of SARS-CoV-2 protein

Anti-COVID-19 antibody was firstly bound with the Au NPs@rPGO modified ITO substrate, and the immobilization was investigated using SERS spectroscopy. The SERS spectrum of the anti-COVID-19 was illustrated in Fig. 2**a** within a range from 500 cm^{-1} to 2000 cm^{-1}. The spectrum indicated the immobilization of the anti-COVID-19 based on the appearance of the SERS bands at 543 cm^{-1} (SS bond of protein), 936 cm^{-1} (α-helix, str. C—C, str. C—N), 1190 cm^{-1} (tryptophan, phenylalanine, str. C—N

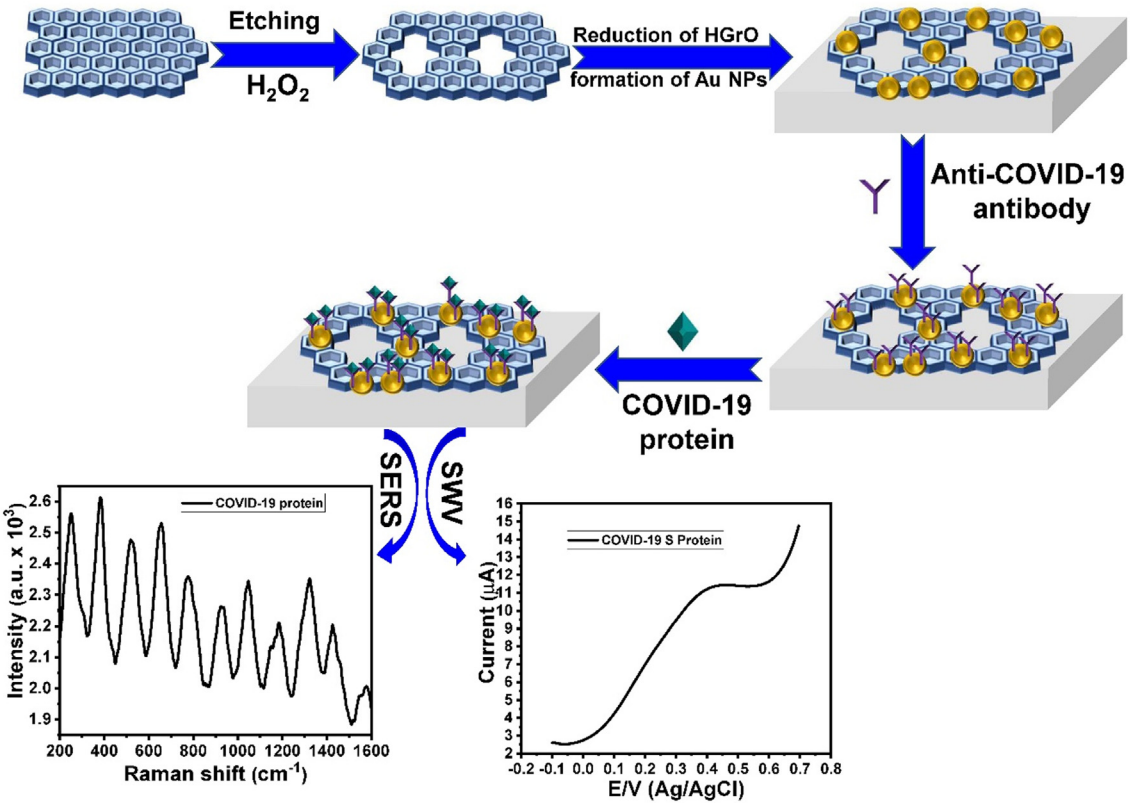

Scheme 1. Schematic diagram of COVID-19 biosensor that including, (i) synthesis of porous graphene oxide, (ii) reduction of porous graphene oxide and deposition of Au NPs onto ITO electrode, (iii) immobilization of antiCOVID-19 antibody, and (iv) capture of COVID-19 protein.

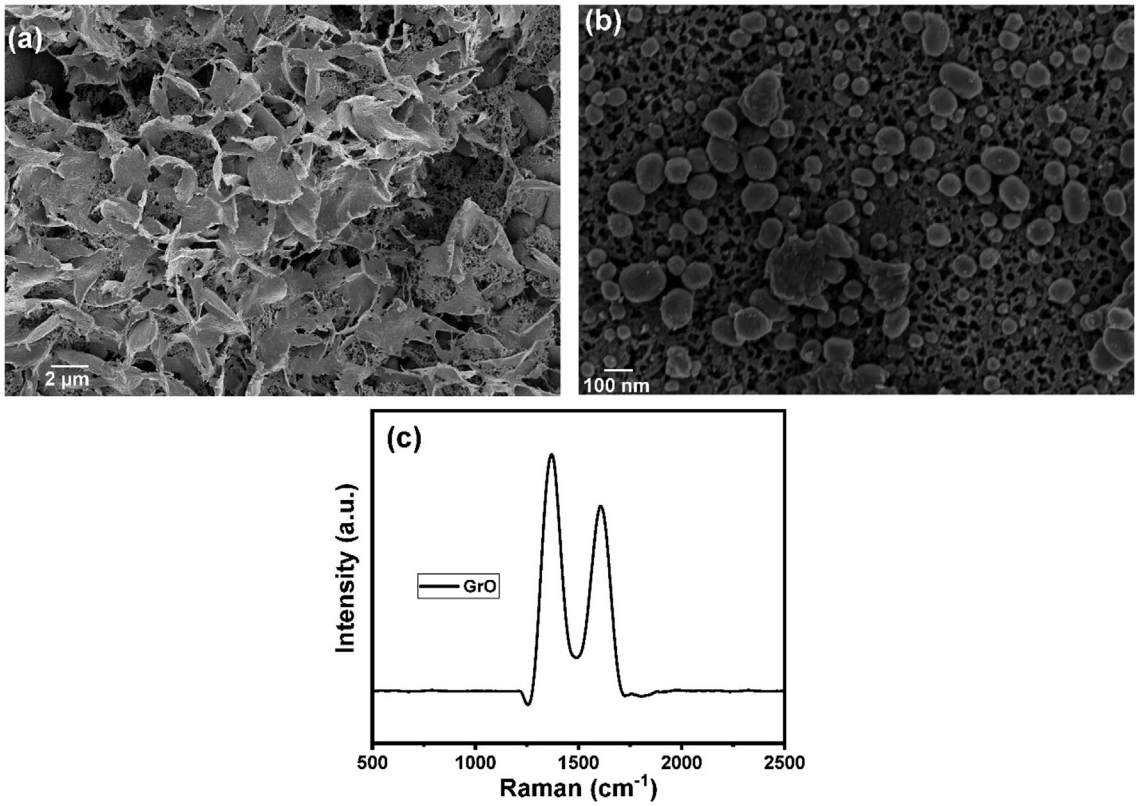

Fig. 1. (a) SEM image of porous graphene oxide sheets, (b) SEM image of Au NPs@reduced porous graphene oxide sheets, and (b) Raman spectrum of Au NPs@reduced porous graphene oxide sheets.

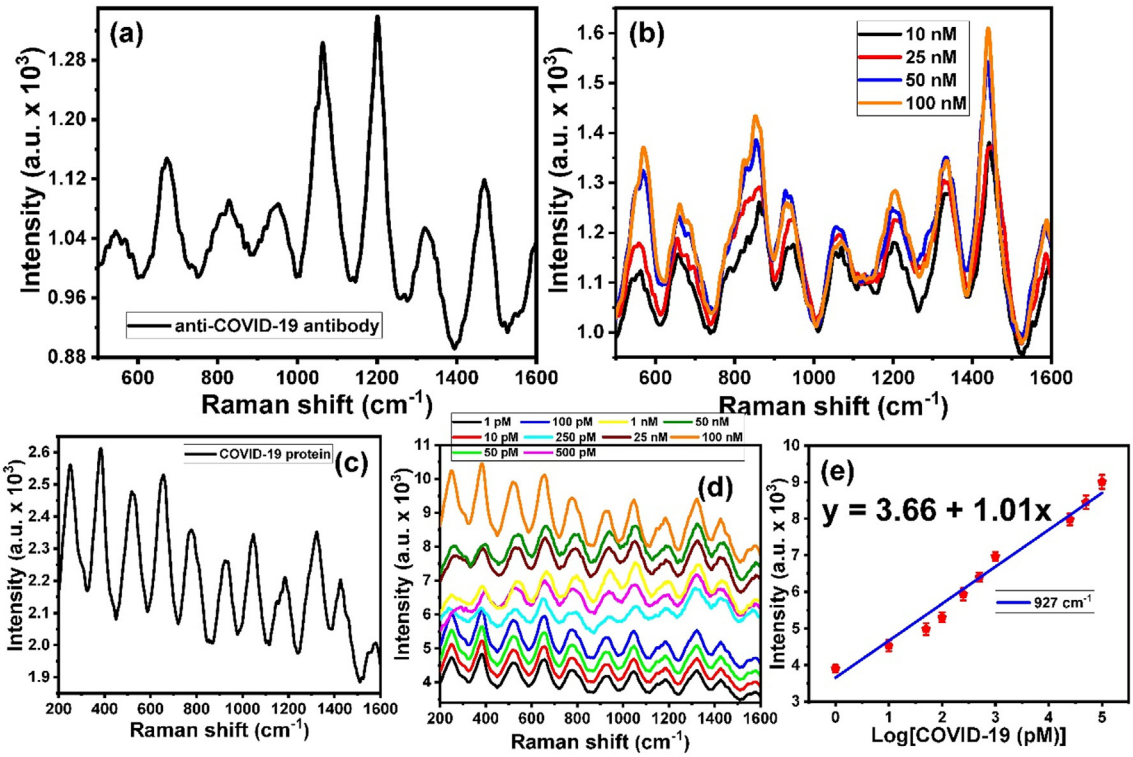

Fig. 2. (a) SERS spectrum of anti-COVID-19 antibody/Au NPs@rPGO modified ITO, (b) SERS spectra of different concentrations of anti-COVID-19 antibody/Au NPs@rPGO modified ITO, (c) SERS spectrum of 100 pmol/L COVID-19 protein/anti-COVID-19 antibody/Au NPs@rPGO modified ITO, (d) SERS spectra of different concentrations of COVID-19 protein within a range from 100 nM to 1 pM, and (e) the relationship between the SERS intensities and the concentrations of the anti-COVID-19 antibody at Raman shift of 927 cm^{-1}.

and bending N—H of Amide III), 1318 cm^{-1} (α-helix, Amide III), and 1448 cm^{-1} (Amide II/N—H bending, C—N stretch, bending CH_2 of proteins) [34-39].

Different amounts of the anti-COVID-19 (from 10 nmol L^{-1} to 100 nmol L^{-1}) were immobilized onto the Au NPs@rPGO modified ITO substrate to study the effect of the anti-COVID-19 antibody. Then, their corresponding SERS spectra were represented in Fig. 2**b** to detect the optimum amount of the anti-COVID-19 antibody. The results showed that the SERS' intensities were increased with increasing the concentration of the anti-COVID-19 antibody until it reached saturation at a concentration of 50 nmol L^{-1}. Hence, we have used this amount for all the further measurements.

After immobilizing the anti-COVID-19 antibody onto the Au NPs decorated rPGO/ITO substrate, a 50 μL of the COVID-19 protein interacted with the anti-COVID-19 antibody for 6 h 4 °C, then washed the substrate with DIW. The capturing of the COVID-19 protein using anti-COVID-19 antibody was monitoring based on the SERS spectrum. The capturing of the COVID-19 protein with the anti-COVID-19 antibody/Au NPs@rPGO modified ITO substrate was confirmed based on the SERS technique (Fig. 2**c**), which showed a set of SERS bands. The assignment of these bands was tabled in Table 1.

To study the efficiency of the developed sensor, the SERS spectra of different concentrations of COVID-19 protein after interaction with anti-COVID-19 antibody immobilized on Au NPs@rPGO modified ITO substrate as shown in Fig. 2**d**. The results indicated the increase of the SERS signals' intensities with increasing the concertation of the COVID-19 protein. The relationship between the COVID-19 protein concentrations and the SERS signals' intensities at Raman shifts 927 cm^{-1} within a concentration range of 100 nM to 1 pM. The results showed a linear plot, as shown in Fig. 2**e**. The limit of detection (LOD) was calculated based on LOD = 3.3*SD/slope, which was 75 fmol L^{-1}.

3.3. Electrochemical detection of SARS-CoV-2 protein

Fig. 3**a** showed the cyclic voltammogram of the bare Au NPs@rPGO modified ITO electrode, which showed no redox peaks. Fig. 3**b** showed the cyclic voltammograms of different concentrations of COVID-19 protein after captured with the anti-COVID-19 antibody/Au NPs@rPGO modified ITO electrode, which illustrated the appearance of two redox peaks, cathodic and anodic peaks at about 0.42 V and 0.52 V, respectively. Furthermore, the results showed that the current peak was increased with increasing the concertation of the COVID-19 protein. The relationship between the COVID-19 protein concentrations and the current peak at 0.52 V (Fig. 3**c**) showed a linear plot within a concentration range from 1 pM to 100 nM.

Fig. 4**a** showed the anodic SWV voltammogram of the anti-COVID-19 antibody/Au NPs@rPGO modified ITO electrode. The results indicated the appearance of a broad and week anodic peak at about 0.2 V. Furthermore, the SWV voltammogram of 100 pM of COVID-19 protein after interacting with the anti-COVID-19 antibody/Au microcuboid electrode displayed an anodic peak at about 0.42 V (Fig. 4**b**).

The SWV voltammograms corresponding to the interaction of different concentrations of COVID-19 protein within a range from 500 fM to 100 nM with an anti-COVID-19 antibody/Au NPs@rPGO modified ITO electrode were studied to investigate the efficiency of the presented sensor (Fig. 4**c**). It was observed that the anodic current peak was increased with increasing the concertation of the COVID-19 protein. Furthermore, the relationship between the anodic current peak and the corresponding COVID-19 protein concentrations exhibited a linear plot with a slope of 6.23 and R^2 of 0.993 (Fig. 4**d**). Therefore, the LOD of the presented sensor was found to be 39.5 fM. Table 2 showed the LOD for several COVID-19 sensors, which indicated although some of the previously reported sensors showed a lower LOD compared with our sensor; however, the present sensor has a good LOD besides its easy-to-use and fast response advantages [40-50].

Table 1
assignments of the Raman bands for COVID-19 protein after capture with the anti-COVID-19 antibody/Au NPs@rPGO modified ITO substrate.

Raman Shift (cm^{-1})	Assignment
518	S-S
651	tryptophan, sidechain/indole ring modes
772	tryptophan, sidechain/indole ring modes
927	α–helix, Backbone skeletal stretch/C—C, C—N stretches
1030	phenylalanine, sidechain/phenyl ring modes
1144 & 1186	tyrosine & phenylalanine (sidechain/indole ring mode)
1323	α–helix, Amide III (C—N stretch) and N—H deformation
1422	Symmetric COO— stretch
1456	Amide II (N—H bending) and C—N stretch
1544 & 1586	Tryptophan and Amide II (indole ring mode)
1680	β-sheet and Amide I (C=O stretch)

3.4. Performance of the developed sensor for monitoring spiked COVID-19 protein

To investigate the efficiency of the developed sensor for monitoring COVID-19 protein in a real sample, we have mixed different concentrations of COVID-19 protein with 50 μg of human serum and detected these mixtures. The mixtures of the COVID-19 protein and the human serum allowed to capture with the anti-COVID-19 antibody immobilized on Au NPs@rPGO modified ITO electrode. Fig. 4**e** showed the SERS spectra of different concentrations of COVID-19 protein after interaction with anti-COVID-19 antibody immobilized on Au NPs@rPGO modified ITO electrode in the presence of human serum. The SERS spectra of the various mixtures of COVID-19 protein and human serum have exhibited a set of SERS signals, especially SERS bands at Raman shifts of 372 cm^{-1}, 518–533 cm^{-1}, 651 cm^{-1}, 724–838 cm^{-1}, 936 cm^{-1}, 946 cm^{-1}, 1038 cm^{-1}, 1086 cm^{-1}, 1288 cm^{-1}, 1314 cm^{-1}, 1413 cm^{-1}, and 1596 cm^{-1}. In addition, these data showed the shifting of some peaks besides the disappearance of the SERS peak at 290 cm^{-1} comparing the SERS spectrum of COVID-19 protein in PBS.

In the present work, the selectivity of the developed sensor is based on two key points (1) the uses of the COVID-19 antibody and (2) the fact that Raman showed fingerprints biochemical composition of the analyzed samples [16]. It is easy to observe the difference between the Raman spectra for COVID-19 in PBS and mixed with the human serum (Figs. 2**c and** 4**e**), which realtered to the presence of other proteins in the serum. However, the characteristics' peaks for the COVID-19 protein were also observed in the presence of the serum. Although we could eliminate the serum's effect by subtracting its spectrum, we have used the raw data to confirm the capability of the Raman spectroscopy to detect COVID-19 in the presence of a complected matrix. Besides, Fig. 4**e** confirmed that the Raman peak intensities were increased with increasing the concentration of the spiked COVID-19 protein. The concentration of COVID-19 protein spiked in human serum was measured based on the intensity of the Raman peak at 927 cm^{-1} and calculate the concentration of the COVID-19 protein based on the calibration curve (Fig. 4**d**). The recovery percentages were investigated and represented in Table 3. The results confirmed that the presented sensor has an excellent recovery percentage of COVID-19 protein in real samples with high sensitivity and selectivity.

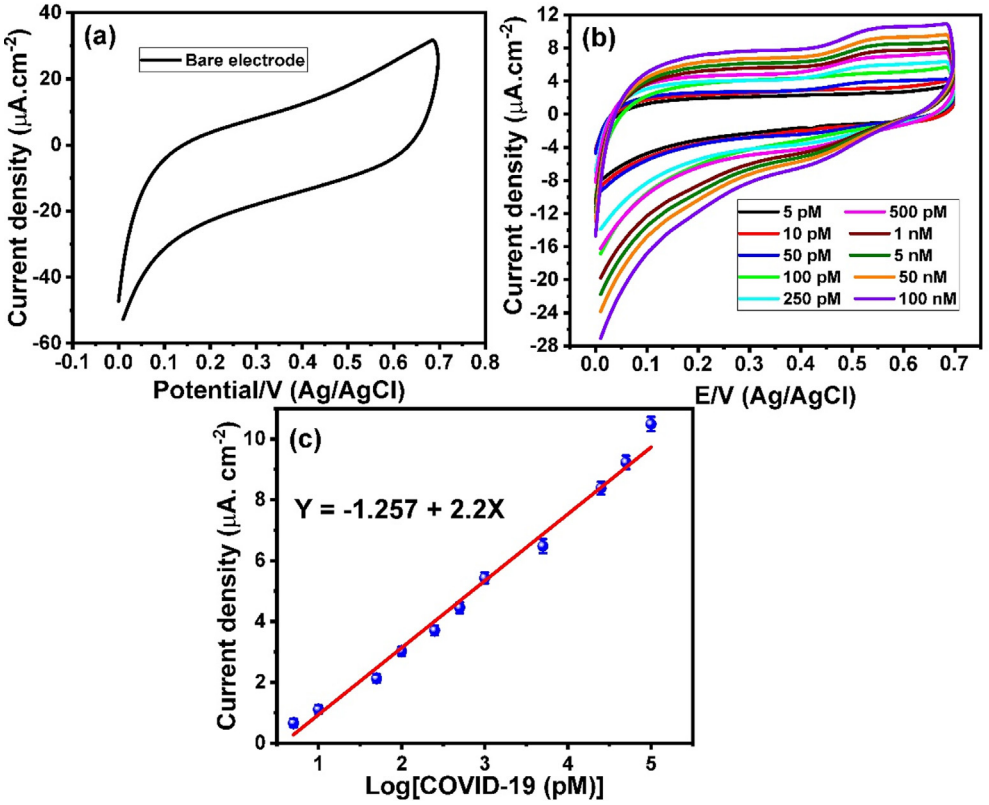

Fig. 3. (a) CV of bare Au NPs@rPGO modified ITO electrode, (b) the CV of different concentrations of COVID-19 protein within a range from 100 nM to 5 pM after interacting with the anti-COVID-19 antibody/Au NPs@rPGO modified ITO electrode, and (c) the relationship between the oxidation current peak and the concentration of COVID-19 protein.

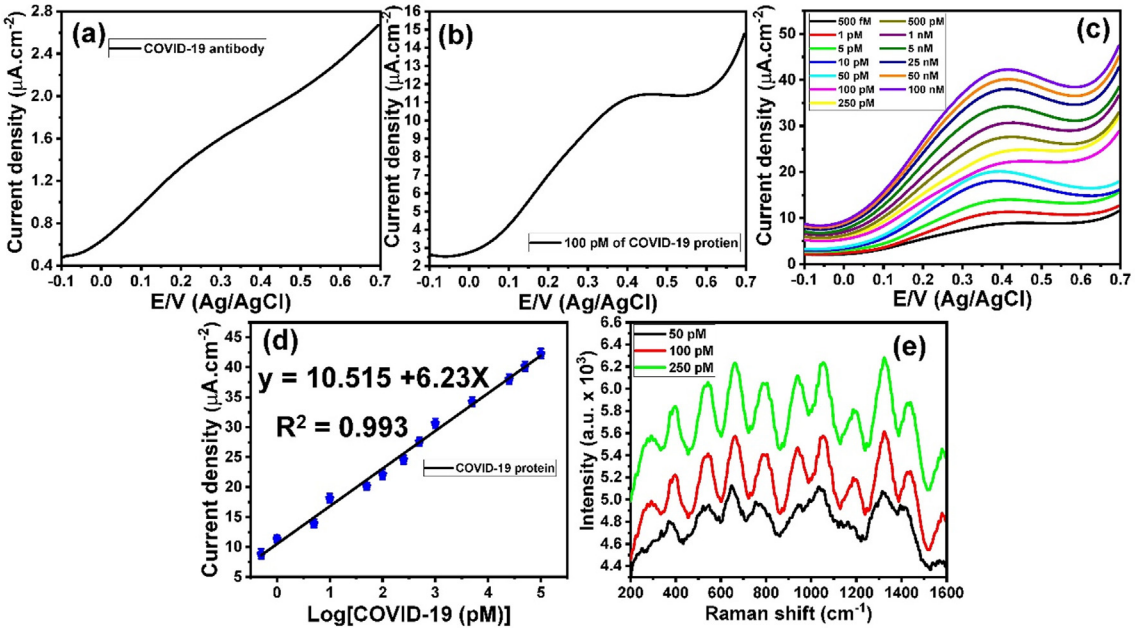

Fig. 4. (a) SWV voltammogram of anti-COVID-19 antibody/Au NPs@rPGO modified ITO electrode, (b) SWV voltammogram of COVID-19 protein after interacting with an anti-COVID-19 antibody/Au NPs@rPGO modified ITO electrode, (c) SWV voltammograms of different concentrations of COVID-19 protein within a range from 100 nM to 500 fM after interacting with the anti-COVID-19 antibody/Au NPs@rPGO modified ITO electrode, (d) the relationship between the oxidation current peak and the concentration of COVID-19 protein, and (e) SERS spectra of three concentrations of COVID-19 protein (50, 100, 250 pM) admixed with human serum.

4. Conclusion

Here, we have successfully fabricated Au NPs decorated rPGO modified ITO based on a simple method. The modification process is based on firstly the fabrication of PGO followed by in-situ reduction of Au^{3+} and PGO. The use of hybrid Au NPs and reduced porous graphene results in enhancing both the Raman effect and the electrochemical conductivity of the developed sensor. This sensor

Table 2
Comparison between the developed sensor and the previously reported COVID-19 sensors.

Sensor	LOD	Reference
Plasmonic metasensors	4.2 fmol L^{-1}	41
Oligonucleotide Capped Plasmonic Nanoparticles	0.18 ng μL^{-1}	42
DNA nanoscaffold hybrid chain reaction	0.96 pmol L^{-1}	43
quantum dot-based	10 ng mL^{-1}	44
SARS-CoV-2 immunodiagnostics kit	250 pg mL^{-1}	45
Electrochemical Impedance Spectroscopy (EIS) (Nanoprinted Reduced-Graphene-Oxide)	2.8 fmol L^{-1}	46
Field-Effect Transistor-Based Biosensor	1 fg mL^{-1}	47
Dual-functional plasmonic photothermal	0.22 pmol L^{-1}	48
Optical biosensor (Au and Ag NPs)	4.2 fmol L^{-1}	49
Square wave voltammetry	39.5 fmol L^{-1}	This work

Table 3
Determination of COVID-19 protein in human serum samples.

Samples	Added (pmol/L)	Found (pmol/L)	RSD (%)	Recovery (%)
1	50	49.64	2.1	99
2	100	103.03	1.7	103
3	250	256.95	1.9	103

showed an excellent capability for monitoring a wide range of concentrations of the COVID-19 protein from 100 nmol L^{-1} to 500 fmol L^{-1} with a detection limit of 39.5 fmol L^{-1}. Finally, mixtures of different concentrations of COVID-19 protein in human serum were detected without needing complicated sample preparation and an excellent recovery percentage.

CRediT authorship contribution statement

Waleed A. El-Said: Conceptualization, Data curation, Formal analysis, Funding acquisition, Methodology, Project administration, Validation, Writing - original draft, Writing - review & editing. **Abdullah S. Al-Bogami:** Conceptualization, Funding acquisition, Writing - original draft, Writing - review & editing. **Wael Alshitari:** Conceptualization, Funding acquisition, Writing - original draft, Writing - review & editing.

Declaration of Competing Interest

The authors declare that they have no known competing financial interests or personal relationships that could have appeared to influence the work reported in this paper.

Acknowledgement

This research is funded by King Abdulaziz City for Science and Technology (KACST), Riyadh, Saudi Arabia (Grant number: 5-20-01-031-0009). We gratefully acknowledge the financial support of the KACST.

References

[1] A.M. Zaki, S. van Boheemen, T.M. Bestebroer, A.D.M.E. Osterhaus, R.A.M. Fouchier, Isolation of a novel coronavirus from a man with pneumonia in Saudi Arabia, N Engl. J. Med. 367 (2012) 1814–1820.
[2] World Health Organization (WHO). Middle East respiratory syndrome coronavirus (MERS-CoV), MERS situation Update November 2019. WHO, 2020. Available from: www.who.int/emergencies/mers-cov/en/ (accessed February 16, 2020).
[3] Ministry of Health (MOH). Command and Control Center. National Public Health Events, 2020. Ministry of Health, 2020.
[4] World Health Organization (WHO). MERS situation update, January 2020. Available from: http://www.emro.who.int/pandemic-epidemic-diseases/mers-cov/mers-situation-updatejanuary-2020.html.
[5] https://www.worldometers.info/coronavirus/
[6] J.-M. Kim, Y.-S. Chung, H.J. Jo, N.-J. Lee, M.S. Kim, S.H. Woo, S. Park, J.W. Kim, H. M. Kim, M.-G. Han, Identification of Coronavirus Isolated from a Patient in Korea with COVID-19, Osong Public Health Res. Perspect. 11 (1) (2020) 3–7.
[7] C. Huang, Y. Wang, X. Li, L. Ren, J. Zhao, Y. Hu, L. Zhang, G. Fan, J. Xu, X. Gu, Clinical features of patients infected with 2019 novel coronavirus in Wuhan, China, Lancet 395 (10223) (2020) 497–506.
[8] F. Cui, H.S. Zhou, Diagnostic methods and potential portable biosensors for coronavirus disease 2019, Biosens. Bioelectron. 165 (2020) 112349.
[9] F. Wu, S. Zhao, B. Yu, Y.-M. Chen, W. Wang, Z.-G. Song, Y. Hu, Z.-W. Tao, J.-H. Tian, Y.-Y. Pei, Nature (2020) 1–5.
[10] J.H. Choi, W.A. El-Said, J.-W. Choi, Highly sensitive surface-enhanced Raman spectroscopy (SERS) platform using core/double shell (Ag/polymer/Ag) nanohorn for proteolytic biosensor, Appl. Surf. Sci. 506 (2020), https://doi.org/10.1016/j.apsusc.2019.144669 144669.
[11] W.A. El-Said, W. Alshitari, J.-W. Choi, Controlled fabrication of gold nanobipyramids/polypyrrole for shell-isolated nanoparticle-enhanced Raman spectroscopy to detect γ-aminobutyric acid, Spectrochim. Acta Part A Mol. Biomol. Spectrosc. (2019) 117890, https://doi.org/10.1016/j.saa.2019.117890.
[12] W.A. El-Said, J.-W. Choi, High selective spectroelectrochemical biosensor for HCV-RNA detection based on a specific peptide nucleic acid, Spectrochim. Acta Part A Mol. Biomol. Spectrosc. 217 (2019) 288–293.
[13] W.A. El-Said, J. Yoon, J.-W. Choi, Nanostructured surfaces for analysis of anticancer drug and cell diagnosis based on electrochemical and SERS tools, Nano Convergence 5 (2018) 11.
[14] W.A. El-Said, T.-H. Kim, Y.-H. Chung, J.-W. Choi, Fabrication of New Single Cell chip to Monitor Intracellular and Extracellular Redox State based on Spectroelectrochemical method, Biomaterials 40 (2015) 80–87.
[15] J.-A. Huang, M.Z. Mousavi, Y. Zhao, A. Hubarevich, F. Omeis, G. Giovannini, M. Schütte, D. Garoli, F. De Angelis, SERS discrimination of single DNA bases in single oligonucleotides by electro-plasmonic trapping, Nat. Commun. 10 (2019) 5321, https://doi.org/10.1038/s41467-019-13242-x.
[16] N. Kim, M.R. Thomas, M.S. Bergholt, I.J. Pence, H. Seong, P. Charchar, N. Todorova, A. Nagelkerke, A. Belessiotis-Richards, D.J. Payne, A. Gelmi, I. Yarovsky, M.M. Stevens, Surface enhanced Raman scattering artificial nose for high dimensionality fingerprinting, Nat. Commun. 11 (2020) 207, https://doi.org/10.1038/s41467-019-13615-2.
[17] G. Demirel, R.L.M. Gieseking, R. Ozdemir, S. Kahmann, M.A. Loi, G.C. Schatz, A. Facchetti, H. Usta, Molecular engineering of organic semiconductors enables noble metal-comparable SERS enhancement and sensitivity, Nat. Commun. 10 (2019) 5502, https://doi.org/10.1038/s41467-019-13505-7.
[18] N. Chen, T.-H. Xiao, Z. Luo, Y. Kitahama, K. Hiramatsu, N. Kishimoto, T. Itoh, Z. Cheng, K. Goda, Porous carbon nanowire array for surface-enhanced Raman spectroscopy, Nat. Commun. 11 (2020) 4772, https://doi.org/10.1038/s41467-020-18590-7.
[19] L. Xie, J. Lu, T. Liu, G. Chen, G. Liu, B. Ren, Z. Tian, Key Role of Direct Adsorption on SERS Sensitivity: Synergistic Effect among Target, Aggregating Agent, and Surface with Au or Ag Colloid as Surface-Enhanced Raman Spectroscopy Substrate, J. Phys. Chem. Lett. 11 (3) (2020) 1022–1029.
[20] M. Asad, A. Zulfiqar, R. Raza, M. Yang, A. Hayat, N. Akhtar, Orange Peel Derived C-dots Decorated CuO Nanorods for the Selective Monitoring of Dopamine from Deboned Chicken, Electroanalysis 32 (1) (2020) 11–18.
[21] M.M. Khalifa, A.A. Elkhawaga, M.A. Hassan, A.M. Zahran, A.M. Fathalla, W.A. El-Said, O. El-Badawy, Highly specific Electrochemical Sensing of Pseudomonas aeruginosa in patients suffering from corneal ulcers: A comparative study, Sci. Reports 9 (2019) 18320, https://doi.org/10.1038/s41598-019-54667-0.
[22] T.-H. Kim, W.A. El-Said, J.H. An, J.-W. Choi, ITO/gold nanoparticle/RGD peptide composites to enhance electrochemical signals and proliferation of human neural stem cells, Nanomed.: Nanotechnol. Biol., Med. 9 (3) (2013) 336–344.
[23] W.A. El-Said, C.-H. Yea, J.-W. Choi, I.-K. Kwon, Ultrathin polyaniline film coated on an indium-tin oxide cell-based chip for study of anticancer effect, Thin Solid Films 518 (2) (2009) 661–667.
[24] J.-W. Shin, K.-J. Kim, J. Yoon, J. Jo, W.A. El-Said, J.-W. Choi, Silver nanoparticle modified electrode covered by graphene oxide for the enhanced electrochemical detection of dopamine, Sensors (Switzerland) 17 (12) (2017) 2771.
[25] R. Li, H. Qi, Y. Ma, Y. Deng, S. Liu, Y. Jie, J. Jing, J. He, X. Zhang, L. Wheatley, C. Huang, X. Sheng, M. Zhang, L. Yin, A flexible and physically transient electrochemical sensor for real-time wireless nitric oxide monitoring, Nat. Commun. 11 (2020) 3207, https://doi.org/10.1038/s41467-020-17008-8.
[26] M. Senel, M. Dervisevic, S. Alhassen, A. Alachkar, N.H. Voelcker, Electrochemical micropyramid array-based sensor for in situ monitoring of dopamine released from neuroblastoma cells, Anal. Chem. 92 (2020) 7746–7753.
[27] W.A. El-Said, J.-H. Lee, B.-K. Oh, J.-W. Choi, Electrochemical sensor to detect neurotransmitter using gold nano-island coated ITO electrode, J. Nanosci. Nanotechnol. 11 (7) (2011) 6539–6543.
[28] Y. Abbas, S. Ali, M. Basharat, W. Zou, F. Yang, W. Liu, S. Zhang, Z. Wu, N. Akhtar, D. Wu, Heteroatom-Doped Carbon Nanoparticle-Ionic Liquid Composites as

Electrochemical Sensors for Uric Acid, ACS Appl. Nano Mater. 3 (11) (2020) 11383–11390.
[29] Z.S. Miripour, R. Sarrami-Forooshani, H. Sanati, J. Makarem, M.S. Taheri, F. Shojaeian, A.H. Eskafi, F. Abbasvandi, N. Namdar, H. Ghafari, P. Aghaee, A. Zandi, M. Faramarzpour, M. Hoseinyazdi, M. Tayebi, M. Abdolahad, Real-time diagnosis of reactive oxygen species (ROS) in fresh sputum by electrochemical tracing; correlation between COVID-19 and viral-induced ROS in lung/respiratory epithelium during this pandemic, Biosens. Bioelectron. 165 (2020) 112435.
[30] K.A. Alamry, M.A. Hussein, J.-W. Choi, W.A. El-Said, Non-enzymatic electrochemical sensor to detect γ-aminobutyric acid with ligand-based on graphene oxide modified gold electrode, J. Electroanal. Chem. 879 (2020) 114789.
[31] J.-H. Choi, T.-H. Kim, W.A. El-said, J.-H. Lee, L. Yang, B. Conley, J.-W. Choi, K.-B. Lee, In situ detection of neurotransmitters from stem cell-derived neural interface at the single-cell level via graphene-hybrid SERS nanobiosensing, Nano Lett., Doi: 10.1021/acs.nanolett.0c03205.
[32] I.I. Althagafi, S.A. Ahmed, W.A. El-Said, Fabrication of gold/graphene nanostructures modified ITO electrode as highly sensitive electrochemical detection of Aflatoxin B1, PLoS ONE 14 (1) (2019), https://doi.org/10.1371/journal.pone.0210652 e0210652.
[33] W.A. El-Said, C.-H. Yea, M. Jung, H.-C. Kim, J.-W. Choi, Analysis of effect of nanoporous alumina substrate coated with polypyrrole nanowire on cell morphology based on AFM topography, Ultramicroscopy 110 (6) (2010) 676–681, https://doi.org/10.1016/j.ultramic.2010.02.031.
[34] D. Yilmaz, H. Mehdizadeh, D. Navarro, A. Shehzad, M. O'Connor, P. McCormick, Application of Raman spectroscopy in monoclonal antibody producing continuous systems for downstream process intensification, Biotechnol Progress. 36 (2020), https://doi.org/10.1002/btpr.2947 e2947.
[35] Z.-Q. Wen, Raman Spectroscopy of Protein Pharmaceuticals, J. Pharm. Sci. 96 (11) (2007) 2861–2878.
[36] L. Ashton, E.W. Blanch, pH-induced conformational transitions in a-lactalbumin investigated with two-dimensional Raman correlation variance plots and moving windows, J. Mol. Struct. 974 (2010) 132–138.
[37] B.S. McAvan, L.A. Bowsher, T. Powell, J.F. O'Hara, M. Spitali, R. Goodacre, A.J. Doig, Raman Spectroscopy to Monitor Post-Translational Modifications and Degradation in Monoclonal Antibody Therapeutics, Anal. Chem. 92 (2020) 10381–10389.
[38] A.E. Baker, A.R. Mantz, M.L. Chiu, Raman spectroscopy characterization of antibody phases in serum, mAbs 6 (6) (2014) 1509–1517, https://doi.org/10.4161/19420862.2014.975100.
[39] I. Ettah, L. Ashton, Engaging with Raman Spectroscopy to Investigate Antibody Aggregation, Antibodies 7 (2018) 24, https://doi.org/10.3390/antib7030024.
[40] A. Ahmadivand, B. Gerislioglu, Z. Ramezani, A. Kaushik, P. Manickam, S.A. Ghoreish, Functionalized terahertz plasmonic metasensors: Femtomolar-level detection of SARS-CoV-2 spike proteins, Biosens. Bioelectron. 177 (2021) 112971.
[41] P. Moitra, M. Alafeef, K. Dighe, M. Frieman, D. Pan, Selective naked-eye detection of SARS-CoV-2 mediated by N gene targeted antisense oligonucleotide capped plasmonic nanoparticles, ACS Nano 14 (6) (2020) 7617–7627.
[42] J. Jiao, C. Duan, L. Xue, Y. Liu, W. Sun, Y. Xiang, DNA nanoscaffold-based SARS-CoV-2 detection for COVID-19 diagnosis, Biosens. Bioelectron. 167 (2020) 112479.
[43] T. Ji, Z. Liu, G.Q. Wang, X. Guo, S.A. khan, C. Lai, H. Chen, S. Huang, S. Xia, B. Chen, H. Jia, Y. Chen, Q. Zhou, Detection of COVID-19: A review of the current literature and future perspectives, Biosens. Bioelectron. 166 (2020) 112455.
[44] P. Mertens, N. De Vos, D. Martiny, C. Jassoy, A. Mirazimi, L. Cuypers, S. Van den Wijngaert, V. Monteil, P. Melin, K. Stoffels, N. Yin, D. Mileto, S. Delaunoy, H. Magein, K. Lagrou, J. Bouze, G. Serrano, M. Wautier, T. Leclipteux, M. Van Ranst, O. Vandenberg and LHUB-ULB, Development and potential usefulness of the COVID-19 Ag Respi-Strip diagnostic assay in a pandemic context. Front. Med. 7 (2020) 225. https://doi.org/10.3389/fmed.2020.00225.
[45] Md.A. Ali, C. Hu, S. Jahan, B. Yuan, M.S. Saleh, Sensing of COVID-19 Antibodies in Seconds via Aerosol Jet Nanoprinted Reduced-Graphene-Oxide-Coated 3D Electrodes, Enguo Ju, Shou-Jiang Gao, and Rahul Panat, Adv. Mater. (2020) 2006647, https://doi.org/10.1002/adma.202006647.
[46] G. Seo, G. Lee, M.J. Kim, S.-H. Baek, M. Choi, K.B. Ku, C.-S. Lee, S. Jun, D. Park, H. G. Kim, S.-J. Kim, J.-O. Lee, B.T. Kim, E.C. Park, S. Il Kim, Rapid Detection of COVID-19 Causative Virus (SARS-CoV-2) in Human Nasopharyngeal Swab Specimens Using Field-Effect Transistor-Based Biosensor, ACS Nano 14 (4) (2020) 5135–5142.
[47] G. Qiu, Z. Gai, Y. Tao, J. Schmitt, G.A. Kullak-Ublick, J. Wang, Dual-functional plasmonic photothermal biosensors for highly accurate severe acute respiratory syndrome coronavirus 2 detection, ACS Nano 14 (5) (2020) 5268–5277.
[48] C. Tymm, J. Zhou, A. Tadimety, A. Burklund, J. Zhang, Scalable COVID-19 detection enabled by lab-on-chip biosensors, Cell. Mol. Bioeng. 13 (2020) 1–17.
[49] B.D. Kevadiya, J. Machhi, J. Herskovitz, M.D. Oleynikov, W.R. Blomberg, N. Bajwa, D. Soni, S. Das, M. Hasan, M. Patel, A.M. Senan, S. Gorantla, J. McMillan, B. Edagwa, R. Eisenberg, C.B. Gurumurthy, P.M. St, C. Reid, L. Chang Punyadeera, H.E. Gendelman, Diagnostics for SARS-CoV-2 infections, Nat. Mater. 20 (2021) 593–605.
[50] F. Wang, J. Yang, R. He, X. Yu, S. Chen, Y. Liu, L. Wang, A. Li, L. Liu, C. Zhai, L. Ma, PfAgo-based detection of SARS-CoV-2, Biosens. Bioelectron. 177 (2021) 112932.